scientific reports

OPEN

NMDAR mediated dynamic changes in m^{6}A inversely correlates with neuronal translation

Naveen Kumar Chandappa Gowda[1,2], Bharti Nawalpuri[2], Sarayu Ramakrishna[2], Vishwaja Jhaveri[1] & Ravi S. Muddashetty[2]✉

Epitranscriptome modifications are crucial in translation regulation and essential for maintaining cellular homeostasis. N6 methyladenosine (m^{6}A) is one of the most abundant and well-conserved epitranscriptome modifications, which is known to play a pivotal role in diverse aspects of neuronal functions. However, the role of m^{6}A modifications with respect to activity-mediated translation regulation and synaptic plasticity has not been studied. Here, we investigated the role of m^{6}A modification in response to NMDAR stimulation. We have consistently observed that 5 min NMDAR stimulation causes an increase in eEF2 phosphorylation. Correspondingly, NMDAR stimulation caused a significant increase in the m^{6}A signal at 5 min time point, correlating with the global translation inhibition. The NMDAR induced increase in the m^{6}A signal is accompanied by the redistribution of the m^{6}A marked RNAs from translating to the non-translating pool of ribosomes. The increased m^{6}A levels are well correlated with the reduced FTO levels observed on NMDAR stimulation. Additionally, we show that inhibition of FTO prevents NMDAR mediated changes in m^{6}A levels. Overall, our results establish RNA-based molecular readout which corelates with the NMDAR-dependent translation regulation which helps in understanding changes in protein synthesis.

m^{6}A is a widespread, abundant and well conserved internal RNA modification, which plays a pivotal role in regulating multitude of physiological and pathological processes. It is present on diverse classes of RNA molecules such as rRNAs, mRNAs, tRNAs, snRNAs, miRNAs, and long non-coding RNAs. In mammalian mRNA, m^{6}A is primarily located near the stop codon, 3' UTR, and long internal exons[1]. It is known to critically regulate several aspects of RNA metabolism, such as RNA stability, splicing, translation, translocation, localization, degradation, and transport[2–4]. This modification is highly enriched in the brain and global levels are developmentally regulated[5].

In mammals, the m^{6}A mark on RNA is dynamically and reversibly regulated by the action of RNA methyltransferases (writers) and demethylases (erasers)[6]. Methyl groups are added co-transcriptionally onto the adenosine nucleotide through a multicomponent methyltransferase complex. This complex consists of a catalytic core protein Methyltransferase-like 3 (METTL3), along with the adaptor proteins Methyltransferase-like 14 (METTL14) and Wilms tumour 1 associated protein (WTAP)[6]. This m^{6}A mark can be reversed by the action of m^{6}A demethylases, Fat mass and obesity-associated (FTO)[7] and alkB homolog 5 (ALKBH5)[8]. These demethylases primarily differ in their substrate preference and localisation. Alkbh5 is localised in the nucleus and demethylates m^{6}A on DRACH motif. Whereas, FTO is localised both in the cytosol and the nucleus and acts on broad spectrum substrates[8]. Some studies have defined the role of FTO in neuron present in cytosol and dendrites, where it regulates local translation of mRNA[9,10]. Thus, these studies provide basis for the FTO to study the role of activity mediated translation response. The m^{6}A mark is recognised by a set of the proteins known as readers, which preferentially binds to the methylated RNA and mediate the downstream effector functions of m^{6}A modification[11]. The YTH domain-containing proteins YTHDF1-3, YTHDC1-2 are the most common m^{6}A readers in mammals, and are proposed to play a role in determining the stability and translational efficiency of the bound transcripts[12–14].

Several recent studies have uncovered the role of m^{6}A modification in the nervous system. The m^{6}A modified transcripts are highly enriched in the brain[5,15], and their levels are developmentally regulated[16,17]. Studies involving knockdown and overexpression of m^{6}A writers and erasers have demonstrated the role of m^{6}A in the process of neurogenesis, axon morphogenesis, synapse morphogenesis and synaptic plasticity[18,19]. Furthermore, studies have also shown the preferential synaptic localization of m^{6}A marked transcripts, and experience dependent

[1]Institute for Stem Cell Science and Regenerative Medicine, Bangalore 560065, India. [2]Centre for Brain Research, Indian Institute of Science, Bangalore 560012, India. ✉email: ravimshetty@iisc.ac.in

Figure 1. NMDAR stimulation leads to increase in m6A levels on RNA which correlates with the global translation inhibition response (**a**) Representative image showing p-eEF2 and MAP2 staining in DIV15 cultured cortical neurons treated with 20 μm NMDA for 1, 5 and 20 min. (**b**) Quantification of p-eEF2 levels normalized to MAP2 in DIV15 cultured cortical neurons treated with 20 μm NMDA for 1, 5 and 20 min. Data represents mean +/− SEM, n > 22 neurons for all groups, from at least 3 independent neuronal cultures, Kruskal- Wallis test followed by Dunn's multiple comparison test. (**c**) Schematic depicting m6A dot blot procedure after 20 μm NMDA treatment in cultured cortical neurons. (**d**) m6A immunoblot and methylene blue (MB) staining blot processed parallelly for the DIV15 cortical neurons treated with 20 μm NMDA for 1, 5 and 20 min. (**e**) Quantification of the m6A immunoblot normalized to MB signal in 20 μm NMDA stimulated neurons. Data represents mean +/− SEM, N = 4 independent neuronal cultures, one way ANOVA with Dunnett's multiple comparison test. (**f**) Representative images showing m6A and MAP2 staining in DIV15 cultured cortical neurons treated with 20 μm NMDA for 1, 5 and 20 min. (**g**) Quantification of m6A levels (normalized to MAP2) in DIV15 cultured cortical neurons treated with 20 μm NMDA for 1, 5 and 20 min. Data represents mean +/− SEM, n > 24 neurons for all groups, from at least 3 independent neuronal cultures, Kruskal- Wallis test followed by Dunn's multiple comparison test. (**h**) Representative immunoblots showing enrichment of PSD95 in synaptoneurosomes (SNS) samples. Sample indicating total lysate and SNS are stained against PSD95 and Tubulin as loading control. (**i**) m6A immunoblot and control methylene blue stained blots processed parallelly for the synaptoneurosomes treated with NMDA (40 μM) for 1, 5 and 20 min. (**j**) Quantification of m6A immunoblot normalized to MB signal for synaptoneurosome samples treated with 40 μm NMDA for 1, 5 and 20 min. Data represents mean +/- SEM, N = 3 animals, One way ANOVA with Tukey's multiple comparison test.

modulation of m6A levels[3]. The dynamic and reversible nature of m6A modifications makes it an excellent candidate for regulation protein synthesis upon synaptic activity. Surprisingly, despite the recent surge in studies focusing on synaptic m6A enrichment and experience dependent m6A modulation, the dynamic regulation of m6A in response to synaptic activity, and its relation to translation remains unexplored[20]. In our previous studies, we have shown the importance of translation regulation[21,22] and its kinetics[23] on synaptic stimulation. In this study, we probed the temporal dynamics of m6A in response to NMDAR stimulation. Briefly, we observe a robust increase in the total m6A levels, temporally coinciding with the global translation inhibition phase of NMDAR stimulation in cultured cortical neurons. This is facilitated by the reduction in the somato-dendritic expression of the m6A demethylase FTO along with the redistribution of m6A marked transcripts in the non-translating fractions of the polysome profile.

Results and discussion

NMDAR stimulation leads to increase in m6A levels on RNA which correlates with the global translation inhibition.
In this study, we have used a well-established NMDAR stimulation paradigm to understand the change in m6A levels on RNA in response to synaptic activity in neurons[24]. NMDAR is known to elicit a dynamic translational response in neurons, involving rapid and robust inhibition of global translation for a short term period (1–5 min), followed by the activation of global translation at delayed period (20 min)[21,23,24]. At first, we validated our NMDAR stimulation paradigm by measuring the translation response in cultured rat cortical neurons upon NMDA treatment for 1, 5, and 20 min. We used the phosphorylation status of eEF2 to measure global translation response downstream of NMDAR stimulation. We measured the levels of p-eEF2 in cortical neurons using immunostaining analysis after 1, 5, and 20 min of treatment with 20 μM NMDA. We observed a robust, threefold increase in p-eEF2 levels upon 1-min NMDAR stimulation (Fig. 1A,B). By 5 min, the p-eEF2 levels had reduced compared to 1 min time point; however, it remained significantly higher compared to unstimulated condition (Fig. 1A,B). By 20 min, there was a maximum reduction in p-eEF2 levels, bringing it lower than the untreated condition (Fig. 1A,B). In addition, we have quantified the phosphorylation of eEF2 through western blotting and we observed a significant increase in p-eEF2 levels at 1 min NMDAR stimulation (Supplementary Figs. 1A and B). These results are in accordance with the previous reports[23,24] which show a rapid translation inhibition followed by a delayed translation activation upon NMDAR stimulation.

Next, to understand the NMDAR mediated changes in m6A kinetics, we used the RNA dot blot method to measure the total m6A levels upon 1, 5 and 20 min of NMDA treatment of cultured cortical neurons. Brief methodology and steps involved in RNA dot blotting are indicated in Fig. 1C. Total RNA samples extracted from the DIV15 cultured neurons treated with NMDA (1,5 and 20 min) are indicated in the dot blot (Fig. 1D). We have also shown that the observed m6A signal is majorly contributed by RNA and not by DNA (Supplementary Fig. 1C). Blots were probed for m6A and methylene blue (colorimetric read out) which was used as a loading control (Fig. 1D). We observed a significant increase in total m6A levels on 5-min and 20 min of NMDAR stimulation, while the 1-min time point did not show any significant change as compared to the untreated condition (Fig. 1D,E). These results suggest that, at 5 min NMDAR stimulation, the increased m6A levels correlate with the translation inhibition (increased phosphorylation of eEF2). Hence, we propose that measured m6A levels are inversely correlative to NMDAR translation response at the 5 min time point. Interestingly, there is a time delay in the peaking of m6A levels (peaks at 5 min) as compared to eEF2 phosphorylation (peaks at 1 min). This indicates that the change in m6A levels is likely to be downstream of the kinase activation upon NMDAR stimulation. Further, measured m6A levels at 20 min shows a decreasing trend compared to 5 min NMDAR stimulation, but remains significantly high in comparison to basal condition. These results suggest that the m6A mark on RNA can be used as a potential marker to understand the temporal profile of NMDAR-dependent translation response.

We further validated our dot-blot results by investigating the NMDAR mediated changes in neuronal m6A levels using immunostaining analysis. Similar to our previous experiment, we stimulated DIV15 cultured cortical

2
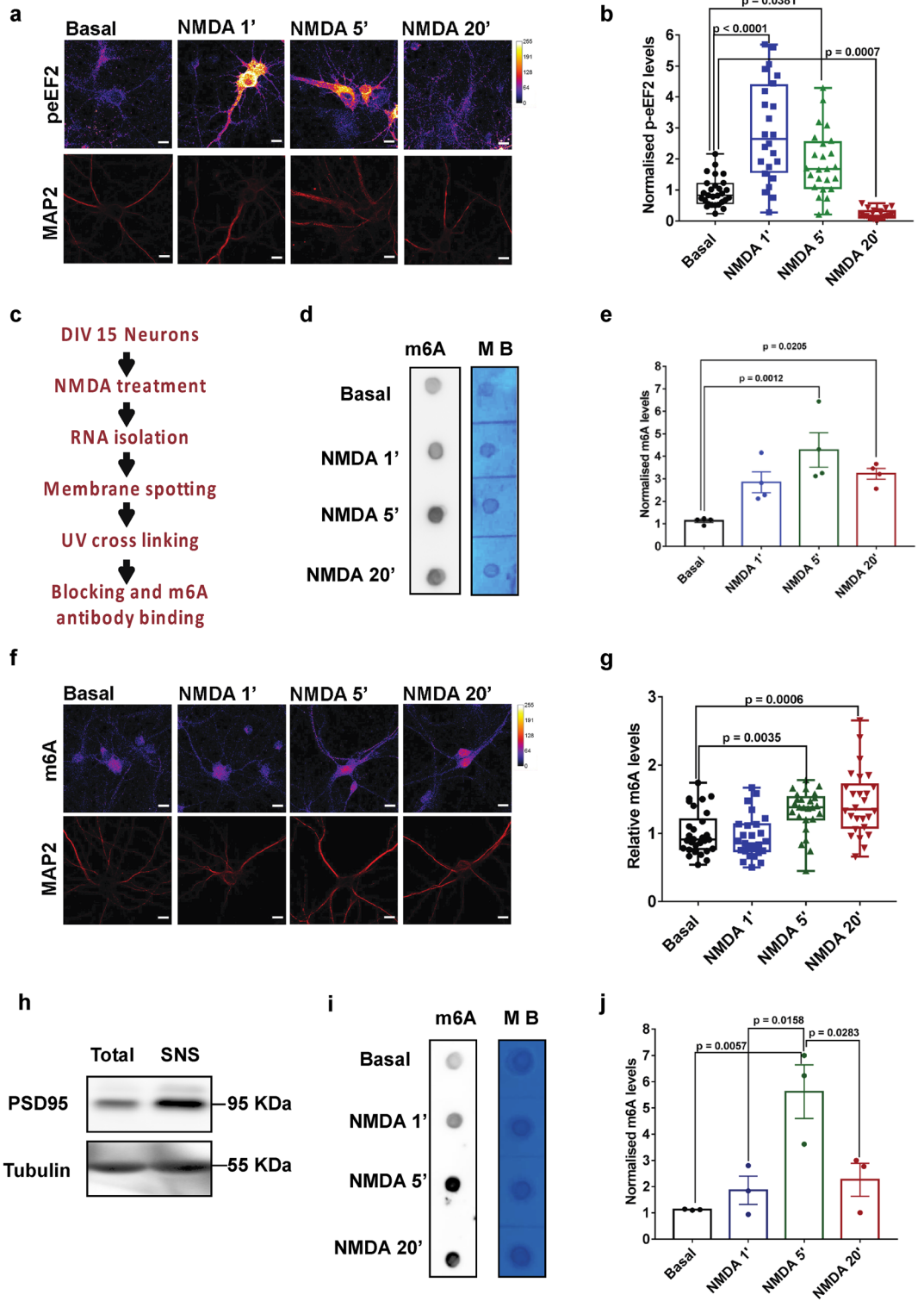
Figure 2. NMDA induces changes in nuclear and cytosolic levels of m[6]A demethylase FTO. (**a**) Representative images showing FTO and MAP2 staining in DIV15 cultured cortical neurons treated with 20 μm NMDA for 1, 5 and 20 min. (**b**) Quantification of cyto-dendritic FTO levels (normalized to MAP2) in DIV15 cultured cortical neurons treated with 20 μm NMDA for 1, 5 and 20 min. Data represents mean +/− SEM, n > 24 neurons for all groups, from at least 3 independent neuronal cultures, Kruskal–Wallis test followed by Dunn's multiple comparison test. (**c**) Representative images showing FTO and MAP2 staining in DIV15 cultured cortical neurons treated with 20 μm NMDA for 1, 5 and 20 min. (**d**) Quantification of mean intensity of nuclear FTO levels in DIV15 cultured cortical neurons treated with 20 μm NMDA for 1, 5 and 20 min. Data represents mean +/− SEM, n > 24 neurons for all groups, from at least 3 independent neuronal cultures, Kruskal- Wallis test followed by Dunn's multiple comparison test. (**e**) FTO immunoblot and control GAPDH blots for the total FTO protein levels treated with NMDA (40 μM) for 1, 5 and 20 min. (**f**) Quantification of FTO levels and plotted values are normalized to GAPDH. Data represent mean +/- SEM, N = 4 independent experiments, One way ANOVA with Tukey's multiple comparison test. (**g**) m[6]A immunoblot for basal and NMDA 5 min condition in presence of FTO inhibitor Meclofenamic acid (MA). (**h**) Quantification of m[6]A signal comparing Basal and MA treatment for 2 h, N = 3, paired T-test. (**i**) Quantification of m[6]A signal in DIV15 cultured cortical neurons treated with 20 μm NMDA for 5 min with and without NMDA, N = 3, paired T-test. (**j**) Quantification of m[6]A signal in DIV15 cultured cortical neurons treated with 20 μm NMDA for 5 min and comparing Basal, N = 3, paired T-test. (**k**) Representation of temporal profiles of eEF2, total m[6]A, and total FTO levels.

neurons with 20 μM NMDA for 1, 5 and 20 min time points followed by immunostaining with m[6]A and MAP2 antibodies. In accordance with our previous results from dot-blot analysis, our image quantification revealed that m[6]A levels were not altered at 1 min, but significantly increased at 5 min and 20 min time points of NMDA treatment (Fig. 1F,G).To validate the total neuronal m[6]A measurements in synaptic compartments, we used synaptoneurosomal preparations. Cortical synaptoneurosomes were prepared from P30 rats and stimulated them with 40 μM NMDA for 1, 5, and 20 min and investigated the changes in m[6]A levels using dot-blot analysis. The synaptoneurosomal preparation was validated by the enrichment of post-synaptic protein PSD95 using immunoblotting analysis (Fig. 1H). We used dot-blot to understand the m[6]A methylation pattern in synapto-neurosomes. Quantification of m[6]A dot blots from synaptoneurosome indicated that m[6]A levels increased upon NMDA treatment, peaking at 5 min time point and showed a significant reduction at 20 min compared to 5 min (Fig. 1I,J). This is consistent with our previous observations from cultured cortical neurons (Fig. 1B,E). Overall, it suggests that NMDAR mediated changes in the m[6]A signal is dynamic and inversely-correlated to translation response (initial increase and later decrease of m[6]A coincides with the initial translation inhibition followed by translation activation), both in the whole neuron and in the synaptic compartments.

NMDAR stimulation induces changes in nuclear and cytosolic levels of m[6]A demethylase FTO.
In the previous section, we showed the distinct temporal profile of m[6]A upon NMDAR stimulation. Next, we wanted to explore the possible mechanism behind NMDAR mediated changes in m[6]A levels. The dynamic changes in m[6]A levels is primarily determined by the action of designated methyltransferases and demethylases[6]. The m[6]A methyltransferases primarily act in the nucleus in a co-transcriptional manner[25], while the m[6]A demethylases are known to function in both nuclear and cytoplasmic compartments[9,26,27]. Since we observed the NMDAR induced changes in the m[6]A levels in the cell body as well as the synapto-dendritic compartments, we hypothesized that m[6]A demethylases are the primary determinant of NMDA-induced changes in m[6]A levels. Among the two widely known m[6]A demethylases, ALKBH5 and FTO, ALKBH5 is known to primarily localize in the neuronal nucleus and its levels are low in the adult brain[26]. On the other hand, FTO is widely studied in neurons and is shown to be expressed in the nucleus, dendrites and dendritic spines of CA1 pyramidal neurons[9]. Hence, we speculated that FTO is the primary driver of mediating NMDAR induced changes in m[6]A levels. To test this, we performed immunostaining to determine the nuclear and cyto-dendritic changes in the FTO levels on 1, 5, and 20 min treatment with 20 μM NMDA. In accordance to the previous studies[9,28], we observed that FTO was primarily localized in neuronal nucleus (Fig. 2A). Notably, we were also able to detect the FTO staining in the cytosolic and dendritic compartments (Fig. 2A). As we find high levels of FTO in the nucleus in comparison to the cyto-dendritic compartment, we imaged nuclear and cyto-dendritic FTO under different imaging parameters (Supplementary Fig. 2A and B). The cyto-dendritic quantification revealed that the levels of FTO significantly decreased upon 1 min NMDAR stimulation and recovered to the basal levels by 5 min time point (Fig. 2B). We did not observe any significant difference in the FTO levels between untreated and 20 min NMDA treated neurons (Fig. 2B). When a similar analysis was done for the nuclear FTO levels, we again found a significant reduction in the FTO levels in 1 min NMDA treated neurons in comparison to the untreated neurons (Fig. 2C,D). However, in contrast to the cyto-dendritic FTO levels, the nuclear FTO levels remained significantly low even after 5 min of NMDA treatment. On 20 min of NMDA treatment, the FTO levels had recovered and was significantly higher compared to the untreated condition (Fig. 2D). To determine the total FTO levels we performed immunoblot on total protein lysate and we observed that significantly low amount of FTO at the 5 min (Fig. 2E,F). Thus, we observed a temporal delay between NMDAR induced reduction in FTO levels versus NMDAR mediated increase in m[6]A levels. A significant and consistent increase in m[6]A levels was observed by 5 min of NMDAR stimulation, whereas the reduction in the total FTO protein levels were consistently low at NMDA 5 min time point.

To understand the importance of FTO in NMDA mediated changes of m[6]A levels, we used an FTO specific inhibitor Meclofenamic acid[29](MA) and compared the m[6]A levels at basal and NMDA stimulation conditions (Fig. 2G). Treatment with MA (120 μmolar) for 2 h caused a significant increase in m[6]A levels compared to
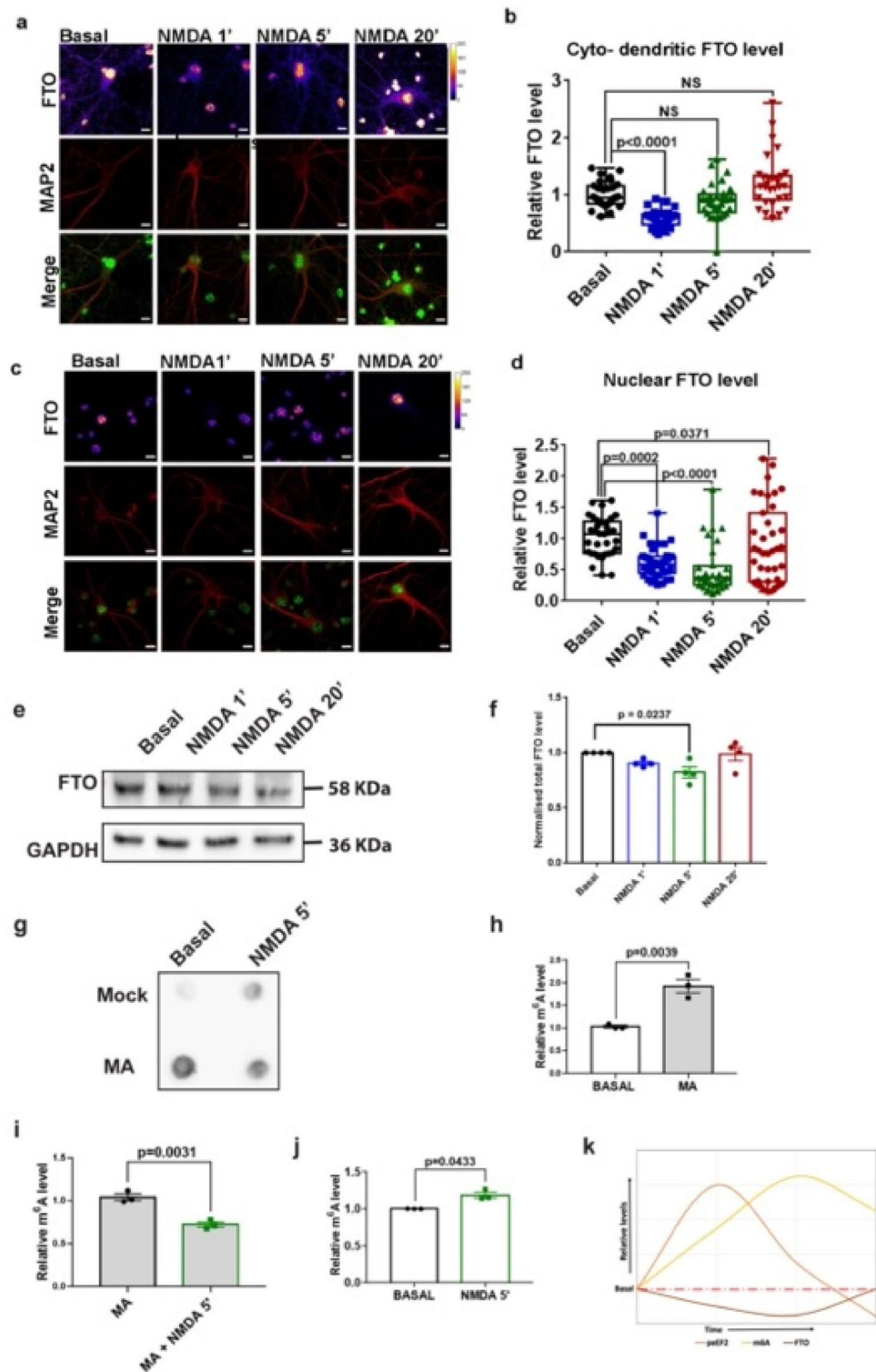
basal condition validating the inhibition of FTO (Fig. 2H). Further, 5-min NMDAR stimulation in the presence of FTO inhibitor MA did cause significant changes in the m6A levels as compared to the mock (MA) treatment (Fig. 2I). Finally, as a control, we recaptured the increase in m6A signal upon 5-min NMDAR treatment in the absence of MA (Fig. 2J). Thus, we show that FTO is a critical player mediating the dynamic changes of m6A levels upon NMDAR stimulation.

In the FTO imaging analysis, we observed differential dynamics of nuclear versus cyto-dendritic changes in FTO levels upon NMDAR stimulation. We speculate that this is primarily caused by redistribution of FTO between these compartments, along with the differential decay kinetics of nuclear and cyto-dendritic FTO. NMDAR induced changes in FTO levels could be attributed to the transcription, translation as well as degradation pathways. We summarise our findings in the representative graph shown in Fig. 2K. The m6A readout follows a similar trend as eEF2 phosphorylation, but with delay in reaching the peak (Fig. 2K). The reduction of the total FTO levels show a good correlation with increase in total m6A levels (Fig. 2K). It is likely that the reduction in the FTO levels on 1 min and 5 min of NMDAR stimulation is caused by ubiquitin-mediated degradation, as NMDAR activation is reported to cause widespread degradation at acute time points[23]. Further, NMDA treatment is also known to cause a delayed translation activation response, providing a possible explanation for the increase in FTO levels on 20 min treatment[23,24].

NMDAR mediated increase in m6A levels is accompanied with the shift of m6A marked RNA from polysome to non-polysome fractions.

Our previous experiments clearly demonstrated the increase in m6A levels upon 5 min of NMDA treatment. From our previous observation, it is known that NMDAR stimulation elicits an overall translation inhibition response at 5 min time point[24]. We wanted to understand if the NMDAR mediated increase in m6A levels drives the translation repression of m6A marked RNAs. To investigate this, we used polysome profiling technique to monitor the distribution of m6A marked RNAs in ribosomal/polysomal pool versus non-ribosomal non-translating pool on NMDA treatment. Briefly, the DIV15 cultured cortical neurons were treated with 20 μM NMDA for 1, 5 and 20 min and the lysates were separated on 15–45% linear sucrose gradient. The steps involved in the sample treatment, polysome profiling and pooling strategy are depicted in Fig. 3A. A representative profile (A254) is shown in Fig. 3B. Additionally, we show the 18S rRNA distribution in the translating and non-translating fractions in the basal condition (Supplementary Fig. 3A).

As shown in schematic Fig. 3B, we have labelled the pooled samples from F1-6 as non-translating and F7-12 as translating pool, indicated in purple and red colour respectively. An equal volume of each fraction was taken for RNA isolation and subjected to dot blot with m6A antibody and methylene blue staining to generate the calorimetric signal (loading control) (Fig. 3C). We observed a uniform staining in methylene blue treated samples, indicating approximately equal loading of RNA on the membrane. We observed a significant increase in m6A levels in the non-translating pool upon 5 min NMDA treatment (Fig. 3D). In contrast, quantification of the translating pool of ribosomes showed a decrease in m6A signal at 5 min of NMDA treatment (Fig. 3E). Further, quantification of the ratio of m6A levels in the translating to non-translating pool showed a significant decrease of the m6A levels at 5 min NMDAR stimulation compared to basal condition (Fig. 3F). This decrease in m6A levels in the translating fractions suggests that the m6A marked pool of ribosomes and mRNAs associated with them have shifted towards the non-translating pool, indicative of translation inhibition. Altogether this data suggests that the NMDAR induced increase in overall m6A signal is accompanied by the redistribution of m6A marked RNA from translating to non–translating fractions. This shift in signal from translating to non-translating pool could potentially be contributed by both rRNA and mRNA and we are yet to identify the factors driving this shift. In contrast, we observe that the m6A levels does not alter significantly at 1 and 20 min of NMDA treatment. Further, since the m6A mark on these RNAs could be potentially removed by demethylases, these RNAs could shift back to the translating pool. Another interesting possibility is that the pool of RNAs present in m6A marked inhibitory complex could be targeted for enzymatic degradation[30,31]. Thus, from our observations, we conclude that m6A signal dynamically distributed across the polysome fractions upon NMDAR stimulation.

Apart from mRNA m6A modification, there are reports suggesting m6A role in non-coding RNA modification and known to affect gene expression[32,33]. Non-coding RNA like microRNA, tRNA, rRNA and lncRNA are m6A methylated and their changes are implied in diseases such as cancer[33,34]. In case of microRNA, presence of m6A is known to reduce the duplex stability between the 3'UTR and miRNA seed region[33,35]. Other prime example is from the rRNA, where 18S and 28S rRNA carry one m6A mark each which is shown to regulate protein synthesis[36]. While our interpretation is mainly focused on m6A modifications on mRNA, we cannot rule out the changes in m6A mark on other RNAs contributing to our results.

Overall, we have shown that m6A levels change dynamically upon NMDAR stimulation. At 5 min NMDAR stimulation, we observe an increase in m6A levels which is correlated with a phase of translation inhibition. Correspondingly, m6A signal is also shifted from the translating fractions towards the non-translating pool at 5 min NMDAR stimulation; further supporting the correlation with translation inhibition. Interestingly, the levels of m6A demethylase FTO is decreased at 5 min NMDAR stimulation which is responsible for the increase in m6A levels. Inhibition of FTO prevents the dynamic changes of m6A levels upon NMDAR stimulation indicating that FTO is a key player in this regulation.

Methods

Ethics statement. The study was carried out in compliance with the ARRIVE guidelines. We performed all the animal work in accordance to the guidelines approved by the Institutional Animal Ethics Committee (IAEC) and the Institutional Biosafety Committee (IBSC), InStem, Bangalore, India. All experiments were performed with a minimum of three independent neuronal cultures. All our experiments were performed with cultured neurons and synaptoneurosomes preparation derived from Sprague Dawley (SD) rats. Rat colonies were main-
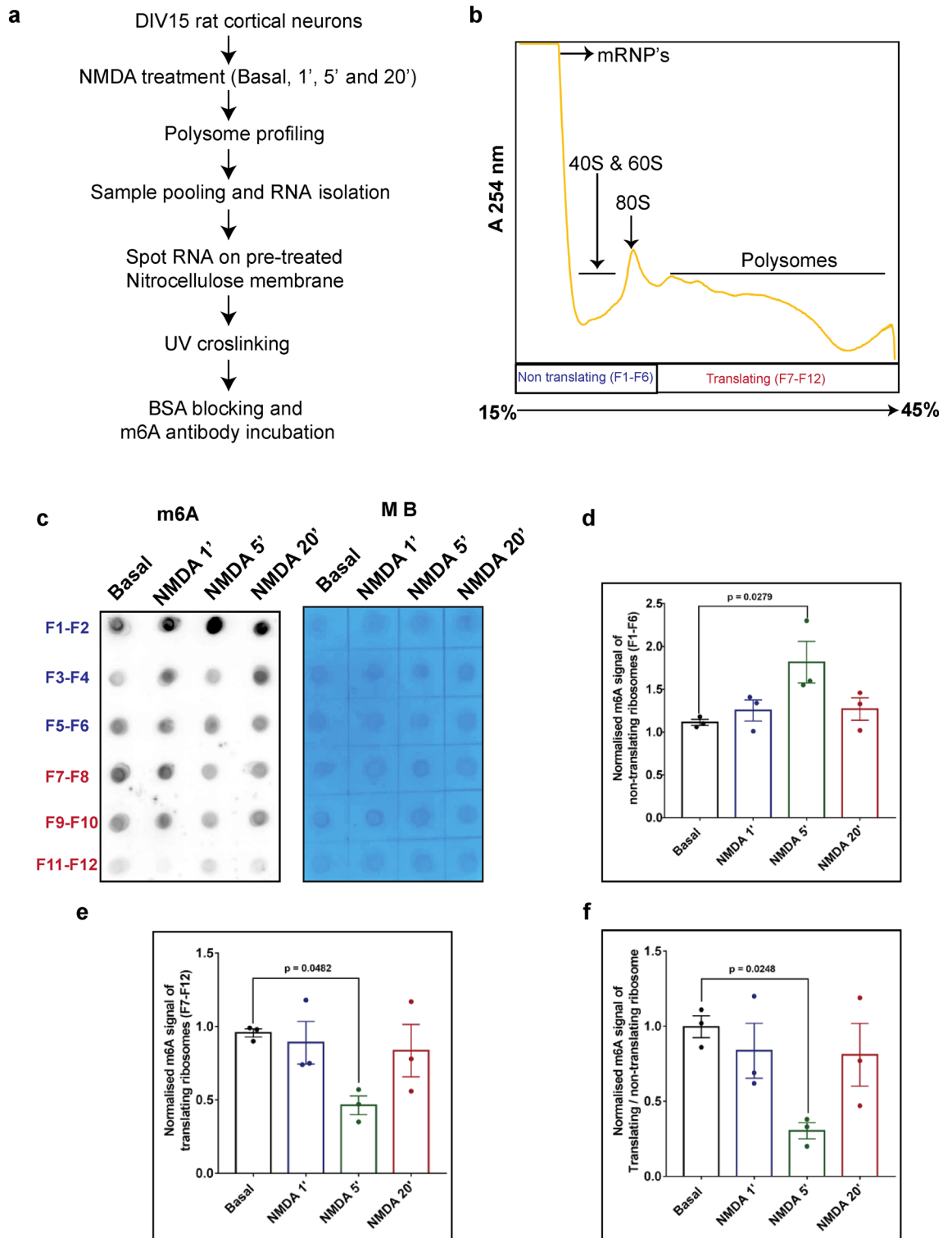
Figure 3. NMDAR mediated increase in m6A levels is accompanied with shift of m6A marked RNA from polysome to non-polysome fractions. (**a**) Schematic representing detailed methodologies for sample preparation, polysome profiling and dot blot to analyze polysome distribution of m6A on 20 μm NMDA treatment. (**b**) Representative polysome profile or absorbance profile (254 nm) run on 15–45% sucrose gradient for the DIV15 rat cortical neurons and sample pooling strategy indicating non-translating pool(in purple) and translating pool (in red). (**c**) m6A dot blot showing pooled polysome fractions on vertical lane and NMDA treatment time points (0, 1, 5 and 20 min) on horizontal lane. Control methylene blue (MB) blots showing the pooled polysome fractions on vertical lane (processed parallelly) and NMDA stimulation time points on the horizontal lane. (**d**) Quantification of m6A signal in non-translating pool of polysome samples obtained from NMDA treated cortical neurons. Data represents mean +/− SEM, N = 3 independent cultures, One way ANOVA with Dunnett's multiple comparison test. (**e**) Quantification of m6A signal in translating pool of polysome samples obtained from NMDA treated cortical neurons. Data represents mean +/− SEM, N = 3 independent cultures, One way ANOVA with Dunnett's multiple comparison test. (**f**) Quantification of the ratio of m6A signal from translating pool to non-translating pool of polysome samples obtained from NMDA treated cortical neurons. Data represents mean +/− SEM, N = 3 independent cultures, One way ANOVA with Dunnett's multiple comparison test.

tained at 14 h/10 h light/dark cycle, 20–22 °C temperature, 50–60% relative humidity. The rooms harbouring the colonies were supplied with 0.3 μm HEPA-filtered air. Rats were freely fed with food and water.

Primary neuronal culture and Inhibitor treatment. Primary neuronal cultures were prepared cortices of embryonic day 18 (E18) Spargue-Dawley rats following previously established protocols[37,38]. Briefly, the dissociated cortices were trypsinised with 0.25% trypsin, followed by washes with sterile HBSS and resuspension in Minimum Essential Media (MEM, 10095080, Thermo Fisher Scientific) containing 10% FBS (F2442, Sigma-Aldrich). The cells were then counted and plated at a density of 40,000 cells/cm^2 on poly-L-lysine (P2636, Sigma-Aldrich) (0.2 mg/ml in borate buffer, pH 8.5) coated dishes. After 3 h of plating, the media was changed to neurobasal (21103049, Thermo Fisher Scientific) supplemented with B27 (17504044, Thermo Fisher Scientific) and Glutamax (35050-061, Life Technologies). Neurons were cultured for two weeks at 37 °C in a 5% CO$_2$ incubator, and supplemented with neurobasal after every five days. On DIV15 the neurons were treated with 20 μM NMDA for 1, 5 and 20 min time points and were processed for downstream experiments as per requirement. FTO Inhibitor-Maclofenamic acid (MA) treatment was done at DIV15 stage at 120 μmolar MA for 24 h and followed by NMDA treatment for 5 min. After treatment with NMDA samples were separated for protein and RNA work.

Immunostaining. NMDA treated DIV15 cortical neurons were fixed with 4% Paraformaldehyde (PFA) for 20 min at room temperature and processed for subsequent immunostaining analysis. Briefly, the fixed neurons were washed with PBS to remove the traces of PFA, followed by 10 min permeabilization with TBS$_{50}$T (0.3%) (50 mM Tris–HCl (pH 7.4), 150 mM NaCl, 0.3% Triton X-100) and 1 h blocking at room temperature with the blocking buffer (TBS$_{50}$T (0.1%), 2% BSA, 2% FBS). Subsequently, the neurons were incubated with required primary antibodies for 2 h at room temperature. Afterwards, the neurons were washed with washes with TBS$_{50}$T (0.1%), and incubated with the required secondary antibodies for 1 h at room temperature. After final washes, the coverslip with neurons were mounted on slide using Mowiol 4–88 mounting media. All the Images were captured on FV3000 confocal microscope (Olympus) at 60X, NA 1.4, oil immersion objective, pinhole set at one airy unit. The imaging parameters were kept constant across different time points in an experiment.

Western blot. DIV15 cortical neurons treated with 20 μM NMDA for different time periods were lysed in lysis buffer containing 50 mM Tris (pH 7.4), 150 mM NaCl, 5 mM MgCl$_2$, 1% Triton X-100, supplemented with EDTA-free protease inhibitor complex (Cat.no- S8830, Sigma) and phosphatase inhibitor cocktail (Cat No. 04906837001, Roche). The cells were subsequently centrifuged at 16,000 RCF for 30 min at 4 °C and the obtained lysates were resuspended in laemmli buffer and were heat denatured at 95 °C for 5 min. The samples were stored at −20 °C until further use. 10% PAGE gel was prepared and 15 μL of sample was loaded onto each well and 1.5 h transfer was done at 4 °C. Blots were stained for the control Ponceaus staining to verify the transfer and after washing blot was blocked for 1 h at room temperature in TBST with 5% BSA. For primary staining we have used total eEF2 (Cat No. 2331S, CST), peEF2 (Cat No. 2332S, CST), FTO (Cat No. 45980, CST) and GAPDH (Cat No. 2118S, CST) as a loading control, secondary antibody (Cat No. A0545, Sigma-Aldrich) with HRP conjugation was used and Clarity western ECL (Bio-Rad) was used to develop and imaged in the GE Amersham imager 600.

For the all the replicative immunoblots of FTO and eEF2 blots were cut at their corresponding molecular weight makers and probed later with respective antibodies. This method of blot imaging was done for simultaneous imaging of blots and to reduce the variance in the assay.

Polysome profiling. The DIV15 rat cortical neurons were stimulated with NMDA (20 μM) for 1, 5 and 20 min. After treatment cells were lysed in lysis buffer (20 mM Tris–HCl, 100 mM KCl, 5 mM MgCl$_2$, 1% NP40, 1 mM dTT, 1X Protease inhibitor cocktail, RNAse inhibitor, 0.1 mg/mL cylohexamide and 1X Phosphotase inhibitor) and centrifuged at 20 K RCF at 4 °C for 20 min. The supernatant was loaded onto 15–45% linear sucrose gradient prepared in buffer (20 mM Tris–HCl, 100 mM KCl, 5 mM MgCl$_2$, 0.1 mg/mL Cycloheximide). The gradient was loaded with cell lysate and centrifuged at 39 K RPM at 4 °C for 90 min. Gradient fractions were collect using Brandel fractionation collector instrument and equal volume of each pooled fractions were processed for RNA isolation and dot blot.

RNA isolation and dot blot. The DIV 15 rat cortical neurons and synaptoneurosomal, RNA was isolated using standard TRIzol RNA extraction method (Thermo Fisher Scientific Cat No. 15596018). Isolated RNA was finally resuspended in milliQ water and its concentration was measured using Qubit (Invitrogen) and equal an concentration of RNA was used for dot blot analysis. For the dot blot, the Nitrocellulose membrane (Cat No. 10600002, Sigma-Aldrich) was cut according to the requirement and rinsed first with milliQ water followed with 20X SSC buffer (Cat.no- AM9763, Thermo Fisher Scientific) and air dried. Extracted RNA was diluted to 250 ng in the RNA dilution buffer (6X SSC buffer and 7.5% para-formaldehyde) and heated to 65 °C for 5 min and kept on ice for 5 min. RNA was spotted on to nitrocellulose membrane and UV crosslinked. The membrane was blocked in TBST with 5% BSA for 1 h at room temperature. Further, membrane was incubated overnight at 4 °C with 1:1000 dilution of m^{6}A antibody (Cat No. 202111, Synaptic systems) Subsequently, the membrane was washed three times in TBST for 10 min of interval. Anti-rabbit-HRP secondary antibody was incubated at 1:10,000 dilution for 1 h at room temperature.

Methylene-blue staining. RNA was extracted from the respective samples using the standard Trizol-LS protocol (Cat No. 10296010, Thermo Fisher Scientific). The Nitrocellulose membrane (Cat No. 10600002, Thermo Fisher Scientific) was cut according to the requirement and rinsed with milli Q water and 10X SSC.

Afterwards the membrane was airdried until the loading of samples. The samples were prepared by diluting the extracted RNA to a final concentration of 250 ng in the RNA dilution buffer followed by heating of diluted samples at 65 °C for 5 min. Afterwards the samples were incubated on ice for 5 min. The diluted RNA sample were spotted on the activated membrane and crosslinked using UV cross linker. After crosslinking, the membrane was incubated with the methylene blue staining solution (0.3 M sodium acetate and 0.03% methylene blue) for 5 min, followed by washes with distilled water to remove the background signal. The processed membrane was then imaged using Image Quant (LAS 4000/Amersham imager 600).

Quantitative PCR.   Isolated RNA from the NMDA treated sample was processed for cDNA synthesis with reverse transcriptase and without reverse transcriptase. 200 ng of RNA was taken and cDNA synthesis was done with random hexamer and while doing the reverse transcription enzyme (M-MLV cat.no 28025013, Invitrogen) was excluded (minus reverse transcription) and included (plus reverse transcription) to the master mix and cDNA synthesis was done according to manufacturer protocol. Quantification of PSD95, PTEN and actin was measured by qPCR using TAKARA SYBR green (Cat.no – RR82WR).

Synapto-neurosome preparation.   Rat cortical synaptoneurosomes were prepared using the filtration method from Sprague Dawley (SD) rat[21,22]. Briefly, the dissected cortices were resuspended in the synaptoneurosome buffer (118 mM NaCl, 5 mM KCl, 1.2 mM $MgSO_4$, 2.5 mM $CaCl_2$, 1.53 mM KH_2PO_4, 212.7 mM Glucose, 1X Protease Inhibitor Cocktail, pH 7.5) followed by homogenization on ice. The obtained homogenate was filtered by passing through three 100 μm nylon filters (NY1H02500, Merck Millipore) and one 11 μm nylon filter (NY1102500, Merck Millipore). The filtrate was then centrifuged at 1500 RCF for 15 min at 4 °C. The pellet obtained was resuspended in 2 mL synaptoneurosome buffer and used for NMDA treatment (40 μM) for different time points. After NMDA treatment, the resuspended synaptoneurosomes were subjected to a brief spin and the obtained pellets were resuspended in lysis buffer (50 mM Tris pH 7.4, 150 mM NaCl, 5 mM $MgCl_2$, 1% Triton X-100, supplemented with EDTA-free protease inhibitor complex and phosphatase inhibitor cocktail) and centrifuged at 16,000 RCF for 30 min at 4 °C. The obtained lysates were used for western blotting and RNA isolation as per previously described protocol.

Statistical analysis.   Statistical analysis was performed using GraphPad prism software version 7.0.0. Prior to the calculation of differences between groups, the data distribution was tested for normality using Kolmogorov Shapiro Smirnov goodness-of-fit test and depending on the distribution, either parametric or non-parametric tests were used to calculate the statistical significance. For groups with less than 5 data points, data distribution was assumed to be normal. Multiple group comparisons were made using one-way ANOVA followed by Bonferroni's multiple comparison test for normally distributed data and Kruskal–wallis followed by Dunn's multiple comparison test. All the tests were doing by using GraphPad Prism version 7.0.0 for Windows, GraphPad Software, San Dieg, California USA, www.Graphpad.com.

References

1. Yue, Y., Liu, J. & He, C. RNA N6-methyladenosine methylation in post-transcriptional gene expression regulation. *Genes Dev.* **29**, 1343–1355 (2015).
2. Knuckles, P. & Bühler, M. Adenosine methylation as a molecular imprint defining the fate of RNA. *FEBS Lett.* **592**, 2845–2859 (2018).
3. Merkurjev, D. *et al.* Synaptic N6-methyladenosine (m6A) epitranscriptome reveals functional partitioning of localized transcripts. *Nat. Neurosci.* **21**, 1004–1014 (2018).
4. Widagdo, J. & Anggono, V. The m6A-epitranscriptomic signature in neurobiology: From neurodevelopment to brain plasticity. *J. Neurochem.* **147**, 137–152 (2018).
5. Meyer, K. D. *et al.* Comprehensive analysis of mRNA methylation reveals enrichment in 3′ UTRs and near stop codons. *Cell* **149**, 1635–1646 (2012).
6. Yang, Y., Hsu, P. J., Chen, Y.-S. & Yang, Y.-G. Dynamic transcriptomic m6A decoration: Writers, erasers, readers and functions in RNA metabolism. *Cell Res.* **28**, 616–624 (2018).
7. Jia, G. *et al.* N6-methyladenosine in nuclear RNA is a major substrate of the obesity-associated FTO. *Nat. Chem. Biol.* **7**, 885–887 (2011).
8. Zheng, G. *et al.* ALKBH5 is a mammalian RNA demethylase that impacts RNA metabolism and mouse fertility. *Mol. Cell.* **49**, 18–29 (2013).
9. Walters, B. J. *et al.* The role of the RNA demethylase FTO (fat mass and obesity-associated) and mRNA methylation in hippocampal memory formation. *Neuropsychopharmacology* **42**, 1502–1510 (2017).
10. Yu, J. *et al.* Dynamic m6A modification regulates local translation of mRNA in axons. *Nucleic Acids Res.* **46**, 1412–1423 (2018).
11. Yen, Y.-P. & Chen, J.-A. The m6A epitranscriptome on neural development and degeneration. *J. Biomed. Sci.* **28**, 40 (2021).
12. Hsu, P. J. *et al.* Ythdc2 is an N6-methyladenosine binding protein that regulates mammalian spermatogenesis. *Cell Res.* **27**, 1115–1127 (2017).
13. Bailey, A. S. *et al.* The conserved RNA helicase YTHDC2 regulates the transition from proliferation to differentiation in the germline. *Elife* **6**, e26116 (2017).
14. Wang, X. *et al.* N(6)-methyladenosine modulates messenger RNA translation efficiency. *Cell* **161**, 1388–1399 (2015).
15. Chang, M. *et al.* Region-specific RNA m⁶A methylation represents a new layer of control in the gene regulatory network in the mouse brain. *Open Biol.* **7**, 170166 (2017).
16. Mathoux, J., Henshall, D. C. & Brennan, G. P. Regulatory mechanisms of the RNA modification m6A and significance in brain function in health and disease. *Front. Cell. Neurosci.* **15**, 671932 (2021).

17. Frye, M., Harada, B. T., Behm, M. & He, C. RNA modifications modulate gene expression during development. *Science* **361**, 1346–1349 (2018).
18. Weng, Y.-L. *et al.* Epitranscriptomic m6A regulation of axon regeneration in the adult mammalian nervous system. *Neuron* **97**, 313-325.e6 (2018).
19. Sokpor, G., Xie, Y., Nguyen, H. P. & Tuoc, T. Emerging role of m6 a methylome in brain development: Implications for neurological disorders and potential treatment. *Front. Cell Dev. Biol.* **9**, 656849 (2021).
20. Yoon, K.-J. *et al.* Temporal control of mammalian cortical neurogenesis by m6A methylation. *Cell* **171**, 877-889.e17 (2017).
21. Kute, P. M., Ramakrishna, S., Neelagandan, N., Chattarji, S. & Muddashetty, R. S. NMDAR mediated translation at the synapse is regulated by MOV10 and FMRP. *Mol. Brain* **12**, 65 (2019).
22. Muddashetty, R. S., Kelić, S., Gross, C., Xu, M. & Bassell, G. J. Dysregulated metabotropic glutamate receptor-dependent translation of AMPA receptor and postsynaptic density-95 mRNAs at synapses in a mouse model of fragile X syndrome. *J. Neurosci.* **27**, 5338–5348 (2007).
23. Ghosh Dastidar, S. *et al.* (2020) Distinct regulation of bioenergetics and translation by group I mGluR and NMDAR. *EMBO Rep.* https://doi.org/10.15252/embr.201948037
24. Ramakrishna, S. *et al.* APOE4 affects basal and NMDAR mediated protein synthesis in neurons by perturbing calcium homeostasis. *J. Neurosci.* https://doi.org/10.1523/JNEUROSCI.0435-21.2021 (2021).
25. Oerum, S., Meynier, V., Catala, M. & Tisné, C. A comprehensive review of m6A/m6Am RNA methyltransferase structures. *Nucleic Acids Res.* **49**, 7239–7255 (2021).
26. Du, T., Li, G., Yang, J. & Ma, K. RNA demethylase Alkbh5 is widely expressed in neurons and decreased during brain development. *Brain Res. Bull.* **163**, 150–159 (2020).
27. Wei, J. *et al.* Differential m6A, m6Am, and m1A demethylation mediated by FTO in the cell nucleus and cytoplasm. *Mol Cell* **71**, 973-985.e5 (2018).
28. McTaggart, J. S. *et al.* FTO Is expressed in neurones throughout the brain and its expression is unaltered by fasting. *PLoS ONE* **6**, e27968 (2011).
29. Huang, Y. *et al.* Meclofenamic acid selectively inhibits FTO demethylation of m6A over ALKBH5. *Nucleic Acids Res.* **43**, 373–384 (2015).
30. Du, H. *et al.* YTHDF2 destabilizes m6A-containing RNA through direct recruitment of the CCR4–NOT deadenylase complex. *Nat. Commun.* **7**, 12626 (2016).
31. Park, O. H. *et al.* Endoribonucleolytic cleavage of m6A-containing RNAs by RNase P/MRP complex. *Mol. Cell* **74**, 494-507.e8 (2019).
32. Meyer, K. D. & Jaffrey, S. R. The dynamic epitranscriptome: N6-methyladenosine and gene expression control. *Nat. Rev. Mol. Cell Biol.* **15**, 313–326 (2014).
33. Fazi, F. & Fatica, A. Interplay between N6-methyladenosine (m6A) and non-coding RNAs in cell development and cancer. *Front. Cell Dev. Biol.* **7**, 116 (2019).
34. Zhao, Y., Shi, Y., Shen, H. & Xie, W. m6A-binding proteins: The emerging crucial performers in epigenetics. *J. Hematol. Oncol.* **13**, 35 (2020).
35. Chen, T. *et al.* m6A RNA methylation is regulated by microRNAs and promotes reprogramming to pluripotency. *Cell Stem Cell* **16**, 289–301 (2015).
36. Sepich-Poore, C. *et al.* The METTL5-TRMT112 N6-methyladenosine methyltransferase complex regulates mRNA translation via 18S rRNA methylation. *J. Biol. Chem.* **298**, 101590 (2022).
37. Kaech, S. & Banker, G. Culturing hippocampal neurons. *Nat. Protoc.* **1**, 2406–2415 (2006).
38. Ravindran, S., Nalavadi, V. C. & Muddashetty, R. S. BDNF induced translation of Limk1 in developing neurons regulates dendrite growth by fine-tuning Cofilin1 activity. *Front. Mol. Neurosci.* https://doi.org/10.3389/fnmol.2019.00064 (2019).

Acknowledgements

Author contributions

N.K.C.G. and R.M. Conceptualise the question, design experiment; N.K.C.G., B.N., V.J. Performed experiments; S.R Provided the resources; N.K.C.G., B.N. and R.M. Analysed data and wrote manuscript.

Funding

Competing interests

The authors declare no competing interests.

Additional information

Supplementary Information The online version contains supplementary material available at https://doi.org/10.1038/s41598-022-14798-3.

Correspondence and requests for materials should be addressed to R.S.M.

Reprints and permissions information is available at www.nature.com/reprints.

Publisher's note Springer Nature remains neutral with regard to jurisdictional claims in published maps and institutional affiliations.